Estimation of Iron Loss Distribution by Image Helmholtz Equation Method

H. Endo, S. Hayano, H. Mogi, M. Fujikura, C. Kaido, and Y. Saito, *Member, IEEE*

Abstract—**This paper proposes the image Helmholtz equation method to visualize iron loss distribution of magnetic materials. The Helmholtz-type equations carry out dynamic image analysis of a series of distinct magnetized domain images. The domain images derive the state transition matrices of which imaginary parts correspond to the phase lag components of magnetization. In the present paper, iron loss distribution of a grain-oriented electrical steel is studied by utilizing its scanning electron microscope (SEM) images. The result of analysis visualizes iron loss generating parts reflecting on the magnetic domains. Moreover, the solution of image Helmholtz equation demonstrates computing magnetization curves, which well agree to experimental result.**

Index Terms—**Grain-oriented electrical steel, image Helmholtz equation method, iron loss, magnetization curve computation, SEM.**

I. INTRODUCTION

A lot of magnetic domain observation methodologies are available to clarify the physics of magnetic material behavior [1]. The understanding of magnetic domain behaviors such as domain structure and boundary displacement leads to the evaluation of magnetic materials. Since the magnetized states can be visualized as the contrast of images, then investigation on microscopy-based measurement such as Kerr effect has been spurred [2]–[4]. Therefore, experts could only accomplish iron loss evaluation based on elaborate analyses. The target of the present paper is to develop a simple means to visualize and to quantify the local iron loss as well as the domain motion dynamics.

We propose a novel dynamic image analysis methodology, i.e., image Helmholtz equation method, to visualize iron loss distribution from a series of distinct magnetized domain images. The image Helmholtz equation is a Helmholtz type of partial differential equations and performs an effective methodology to process the digital dynamic images [5]. Its state transition matrix equivalently represents the characteristic values of physical dynamic system visualized by finite number of images as an animation. In this magnetic domain image analysis, assuming the averaged contrast of domain image as an entire flux density B leads that the characteristics of domain motion deduces from the state transition matrix.

In the present paper, a series of scanning electron microscope (SEM) domain images of a grain-oriented electrical steel is studied to take into account the domain structure in depth of the specimen. The imaginary parts of the state transition matrix visualize iron loss generating parts. The solutions of image Helmholtz equation reproduce the magnetization curves in any magnetized state. As a result, comparison between computed and experimented magnetization curves verifies our methodology.

II. IMAGE HELMHOLTZ EQUATION FOR DOMAIN ANALYSIS

A. SEM Domain Images

Fig. 1 shows the SEM domain images of a grain-oriented electrical steel under the distinct magnetized states [6]. The specimen is the ORIENTCORE·HI-B (Nippon Steel Corporation product) without surface coating and its thickness is 0.23 mm. The backscattered electron observation (Type-II) is carried out at 160-kV acceleration voltage. At this condition, the domain patterns about 10 μm depth from the surface of specimen could be visualized as shown in Fig. 1 [7]. The external field is applied to rolling direction with sloping excitation. The conditions of domain image measurement used in this paper are listed in Table I.

B. Image Helmholtz Equation

To analyze the domain images, we propose a Helmholtz-type equation. The principal idea is that a pixel constituting the digital image is regarded as a scalar potential. Namely, suppose that a domain image as Fig. 1 consists of a two-dimensional (2-D) scalar field U, and then the dynamics of domains can be represented by the image Helmholtz equation [5].

In magnetized state, since the domain motion is caused by applied external field H, then the image Helmholtz equation takes into account a derivative term of the applied external field H

$$\nabla^2 U + \varepsilon \frac{\partial U}{\partial H} = -\sigma \tag{1}$$

where ε and σ, respectively, denote a domain motion parameter and an image source density given by the Laplacian of final image U_{Final} in (2) [8].

$$\nabla^2 U_{\text{Final}} = -\sigma \tag{2}$$

Therefore, the first and second terms on the left-hand side (LHS) in (1) express the spatial expanse and transition of image to the variable H, respectively.
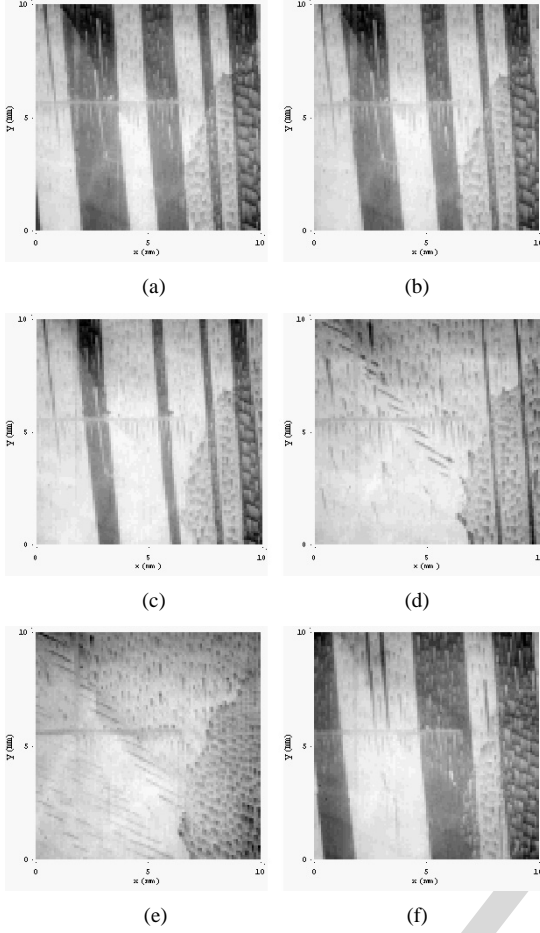
Fig. 1. Magnetic domain images of a grain-oriented electrical steel observed by high-voltage SEM (100 × 100 pixels, 0.1 mm/pixel). (a)–(f) are the domain images numbered as 1, 2, 3, 4, 10, and 19 in Table I, respectively. y direction is the rolling direction and applied external field axis.

In (1), the parameter ε is unknown. Calculation of the parameter ε is the key to visualize the characteristic of domain motion dynamics as well as iron loss generating parts.

C. General Solution

Discretization of (1) using pixel arrangement as nodal points derives the system of equations. The modal analysis of (1) gives a general solution [5]

$$U(H) = \exp(-\Lambda H)(U_{\text{Start}} - U_{\text{Final}}) + U_{\text{Final}} \quad (3)$$

where U_{Start} and Λ are an initial image and a diagonal state transition matrix, respectively. Because of the parameter ε in (1), the state transition matrix is unknown as well. This means that we have to determine the state transition matrix from the given domain images shown in Fig. 1.

D. State Transition Matrix

If we have the solution $U(H)$, then modifying (3) yields the elements in the matrix Λ

$$\Lambda = -\frac{1}{H} \ln \left(\frac{U(H) - U_{\text{Final}}}{U_{\text{Start}} - U_{\text{Final}}} \right) \quad (4)$$

Since the matrix Λ is a diagonal matrix, then (4) is carried out at each corresponding pixel value of three distinct domain images.

TABLE I
CONDITIONS OF OBSERVED SEM DOMAIN IMAGES H: EXTERNAL MAGNETIC FIELD INTENSITY, B: FLUX DENSITY

Image No.	H(A/m)	B(T)	Image No.	H(A/m)	B(T)
1	0.00	0.00	13	214.13	1.93
2	2.85	0.10	14	160.37	1.92
3	9.26	1.63	15	98.68	1.91
4	24.16	1.73	16	54.66	1.84
5	30.23	1.78	17	28.53	1.83
6	54.59	1.84	18	3.73	1.77
7	84.92	1.86	19	0.00	1.73
8	115.39	1.88	20	-4.60	1.73
9	160.69	1.90	21	-5.95	-0.06
10	236.32	1.92	22	-7.45	-1.43
11	324.31	1.95	23	-9.07	-1.56
12	269.64	1.95	24	-11.50	-1.62

Thereby, the elements in the ith matrix Λ_i are determined from a set of three sequential domain images

$$\Lambda_i = \frac{1}{H_{i+1} - H_i} \ln \left(\frac{U_{i+1} - U_{i+2}}{U_i - U_{i+2}} \right), i = 1, 2, \dots, 22. \quad (5)$$

The subscript i refers to a domain image numbered in Table I. The domain images U_i and U_{i+2} correspond to U_{Start} and U_{Final} in (4), respectively. Finally, substituting (5) into (3) gives the solution with piecewise linear approximation.

E. Principle of Iron Loss Visualization

As is well known, the state transition matrix of state variable equations represents the physical parameters and/or constants of the dynamic systems. Similarly, the state transition matrices Λ_i derived from a series of domain images by means of (5) is possible to extract the parameters representing domain dynamics of magnetization region from H_i to H_{i+1}. Due to a logarithmic function in (5), we have to discuss various cases of the element in the matrices Λ_i. Let us consider (6), which is the value under the logarithmic function in (5)

$$f_i = \frac{U_{i+1} - U_{i+2}}{U_i - U_{i+2}} \quad (6)$$

1) *Case 1:* $f_i \geq 1$

The logarithmic function takes a positive real number or zero. Such an element in the matrices Λ_i just represents attenuation or no change term even though (1) is held.

2) *Case 2:* $0 < f_i < 1$

The logarithmic function takes a negative real number. Such an element in the matrices Λ_i represents divergence term.

3) *Case 3:* $f_i = 0$

The logarithmic function becomes indeterminate. This means that the pixel values U_{i+1} and U_{i+2} are identical not holding (1), i.e., the pixel value takes a constant during the state transition.

4) *Case 4:* $0 > f_i > -1$

The logarithmic function takes a complex number composing of the negative real and positive imaginary parts.

This imaginary part means the phase lag to the variable H. Thus, iron loss can be visualized in this case.

5) *Case 5:* $f_i \leq -1$

The logarithmic function takes a complex number composing of the positive real and imaginary parts or a pure positive imaginary part. This complex number means the phase lag to the variable H. Thereby, iron loss can be visualized the same as *Case 4*.

III. RESULTS AND DISCUSSIONS

A. Iron Loss Visualization

Fig. 2 shows the elements in the matrices Λ_i. The arrangement of the elements is the same as the domain pattern in Fig. 1. The elements become complex numbers due to the logarithmic function in (5) as described in Section II-E. The real and imaginary parts, respectively, represent in-phase and 90° difference phase components to the applied field. Namely, visualization of iron loss generating parts can be accomplished by the imaginary part of the matrices Λ_i.

At first, let us consider the real parts of the matrices Λ_i in Fig. 2. In the weak field, the moving parts of the negatively magnetized parts (black parts in Fig. 1) relatively take larger in value. This magnetization process is mainly carried out by the magnetic boundary displacements [LHS of Fig. 2(a)] and magnetic domain movements [LHS of Fig. 2(b)]. Increasing the field, the magnetization process by domain movement is finished. The elements in the matrices Λ_i correspond to the rotation of magnetization [LHS of Fig. 2(c)–(e)]. In highly magnetized state, the elements shown in the LHS of Fig. 2(f) takes relatively small in value due to saturation.

Second, consider the imaginary parts of the matrices Λ_i in Fig. 2. In the weak field, the real part of this region corresponds to the magnetic boundary displacement. However, in case of imaginary part, the elements in the right side of Fig. 2(a) are close to zero. This means that the magnetic boundaries move without delay components. In the right sides of Fig. 2(b) and (c), the values represent at the grain boundary. This is considered to be the friction among the grain boundaries. Increasing the field results in the closure domains. In this region, these elements are then related to iron loss [right sides of Fig. 2(d) and (e)]. Moreover, in highly magnetized state as in Fig. 2(f), magnetization proceeds at the closure domains although the saturation. The iron loss in this region can be visualized at these kinds of domain parts.

B. Major Magnetization Curve

Substituting the matrices Λ_i of (5) into (3) yields domain images as the solution $U(H)$. Computing the averaged contrast of an entire domain image gives a flux density. Fig. 3 shows the computed magnetization curve. Even though the domain images represent a limited area of the specimen, the experimental magnetization curve is close to the computed result.

C. Local Magnetization Curves

Focusing on the particular points on the domain images, it is possible to generate the local magnetization curves as shown in
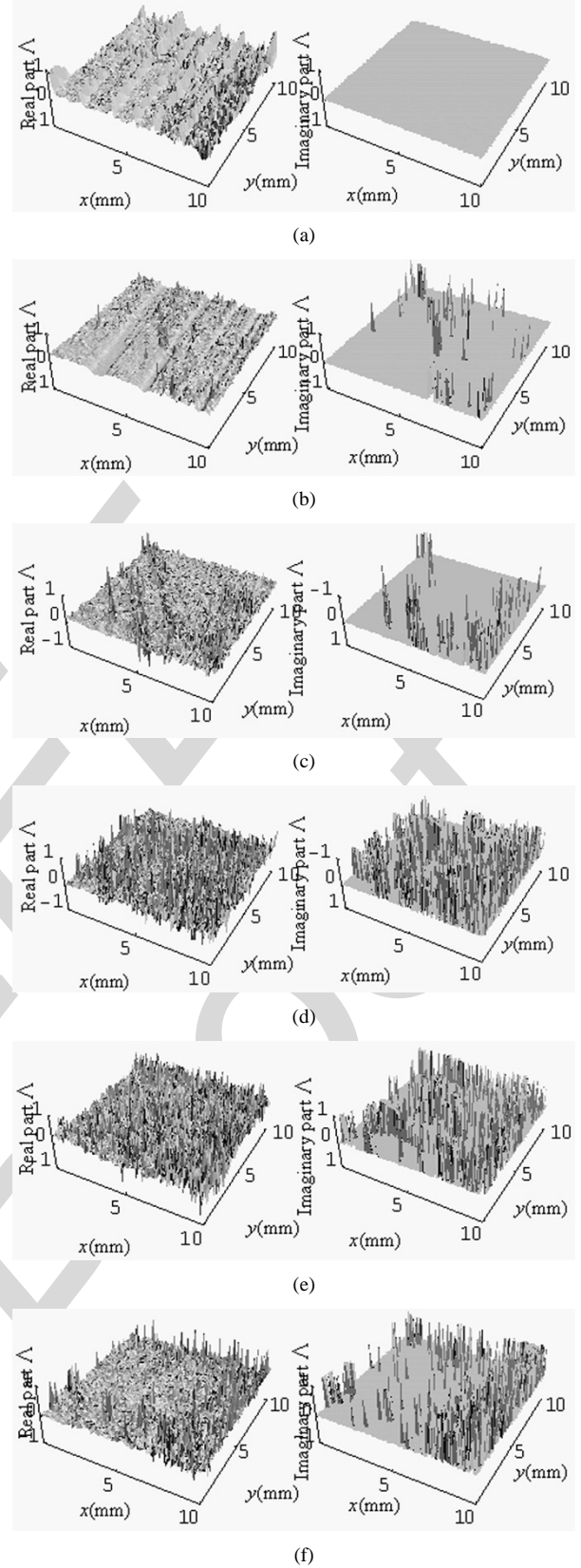

Fig. 2. Elements of the state transition matrices derived from (5). The left and right columns are real and imaginary parts, respectively. The elements are normalized by each maximum value. (a) Λ_1 : H : $0.0 \rightarrow 2.85$ A/m, B : $0.0 \rightarrow 0.10$ T. (b) Λ_2 : H : $2.85 \rightarrow 9.26$ A/m, B : $0.10 \rightarrow 1.63$ T; (c) Λ_4 : H : $24.16 \rightarrow 30.23$ A/m, B : $1.73 \rightarrow 1.78$ T; (d) Λ_6 : H : $54.59 \rightarrow 84.92$ A/m, B : $1.84 \rightarrow 1.86$ T; (e) Λ_7 : H : $84.92 \rightarrow 115.39$ A/m, B : $1.86 \rightarrow 1.88$ T; (f) Λ_9 : H : $160.69 \rightarrow 236.32$ A/m, B : $1.90 \rightarrow 1.92$ T.
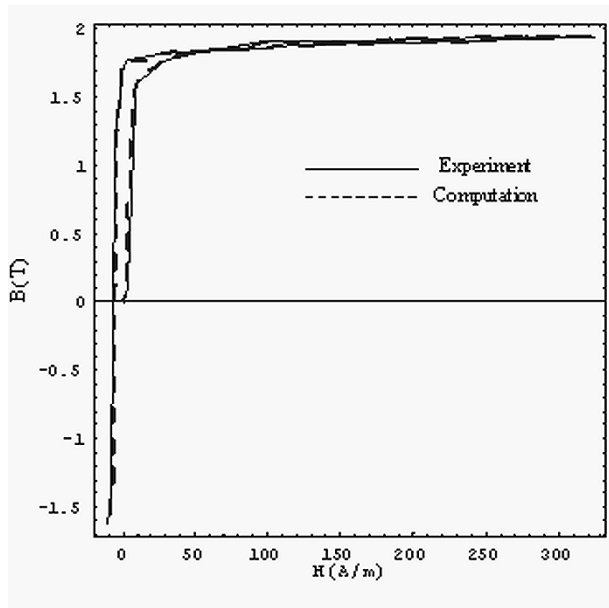
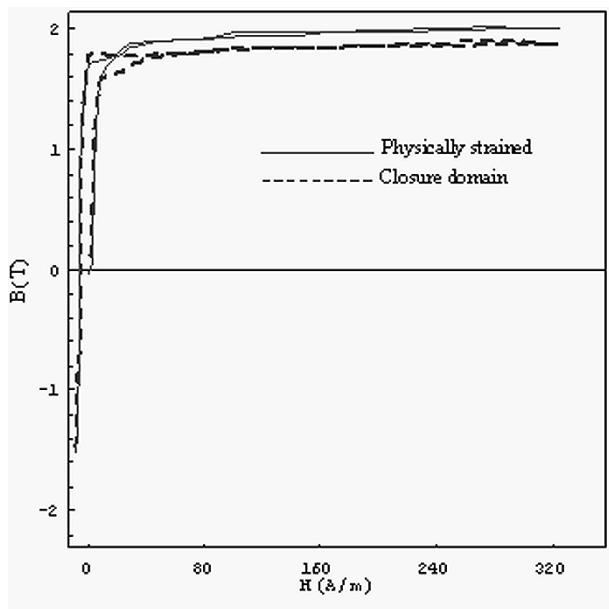Fig. 3. Magnetization curves reconstruction by means of (3).

Fig. 4. Local magnetization curves. Plotted points are shown in Fig. 5.

Fig. 4. Fig. 5 shows the selected parts for drawing local magnetization curves. The local magnetization curve in this methodology is based on that of entire specimen. Our methodology makes it possible to estimate the magnetization processes reflecting on the physical condition of the specimen.
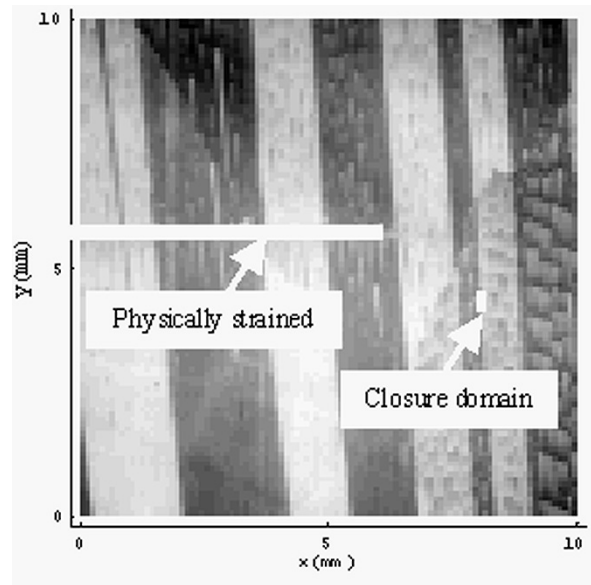

Fig. 5. Selected parts to calculate the local magnetization curves in Fig. 4.

IV. CONCLUSION

This paper has proposed a method of iron loss visualization from a series of distinct domain images. The evaluated state transition matrices derived from the image Helmholtz equation enable us to visualize magnetization processes on the domain images. Since the imaginary part of the state transition matrix corresponds the 90° phase different components to the applied field, and then iron loss generating parts have been visualized in particular. As a result of comparison with conventional measurement, we have succeeded in reproducing the magnetization curve with fairly good accuracy.

REFERENCES

[1] A. Hubert and R. Schäfer, *Magnetic Domains*. Berlin, Germany: Springer-Verlag, 2000.
[2] J.-P. Jamet *et al.*, "Dynamics of the magnetization reversal in Au/Co/Au micrometer-size dot arrays," *Phys. Rev. B*, vol. 57, no. 22, pp. 14 320–14 331, 1998.
[3] S.-B. Choe and S.-C. Shin, "Magnetization reversal dynamics with sub-micron-scale coercivity variation in ferromagnetic films," *Phys. Rev. B*, vol. 62, no. 13, pp. 8646–8649, 2000.
[4] M. Takezawa and J. Yamasaki, "Dynamic domain observation in narrow thin films," *IEEE Trans. Magn.*, vol. 37, pp. 2034–2037, July 2001.
[5] H. Endo, S. Hayano, Y. Saito, and T. L. Kunii, "A method of image processing and its application to magnetodynamic fields" (in Japanese), *Trans. Inst. Elect. Eng. Japan* , vol. 120-A, no. 10, pp. 913–918, 2000.
[6] T. Nozawa, T. Yamamoto, Y. Matsuo, and Y. Ohya, "Effects of scratching on losses in 3-percent Si-Fe single crystals with orientation near (110)[001]," *IEEE Trans. Magn.*, vol. MAG-15, pp. 972–981, Mar. 1979.
[7] K. Tsuno and T. Yamamoto, "Observed depth of magnetic domains and their walls in scanning electron microscopy," *Phys. Stat. Sol. (A)*, vol. 37, pp. 437–448, 1976.
[8] H. Endo, S. Hayano, Y. Saito, and T. L. Kunii, "Image governing equations and its application to vector fields" (in Japanese), *Trans. Inst. Elect. Eng. Japan*, vol. 120-A, no. 12, pp. 1089–1094, 2000.